Calibration of Langmuir probes against microwaves and plasma oscillation probes

Francis F Chen, John D Evans and Wade Zawalski

Electrical Engineering Department, University of California, Los Angeles, CA 90095, USA

Abstract

The use of Langmuir probes for measuring plasma density is subject to uncertainty because the theories commonly used to interpret the data give widely differing results. This is especially troublesome in partially ionized plasmas used, for instance, in the semiconductor industry, since no existing theory adequately treats the case when there are a few collisions between ions and neutral atoms. In this work, plasma densities measured by microwave interferometry and plasma-oscillation probes are compared with those from probe data analyzed with Langmuir's orbital motion limited (OML) theory, the Allen–Boyd–Reynolds (ABR) theory and the Bernstein–Rabinowitz–Laframboise (BRL) theory. It is found that ABR underestimates and BRL overestimates the density, the problems being the neglect of ion orbiting in ABR and the effect of ion-neutral collisions in BRL. The best theory is either OML or the geometric mean between the ABR and BRL results. For thicker probes, other methods are suggested.

(Some figures may appear in colour only in the online journal)

1. Background

Electrostatic probes, appropriately named after Langmuir, are the simplest method to measure local values of plasma density n and electron temperature T_e. The general technique has been described in various books [1–4] and will not be reviewed here. Electron temperature can be obtained from a semi-logarithmic plot of the electron current collected by the probe. Plasma density can be obtained by the ion saturation current I_{sat}, and the interpretation of I_{sat} is the subject of this paper. Here electron and ion densities are assumed to be equal in all plasmas of consequence. In principle, electron density can also be obtained from the electron saturation current, but we do not use this datum because that current can be altered by collisions and stray fields in practical plasmas.

In 1926 Mott–Smith and Langmuir [5] calculated the ion current $I_i(V_p)$ at negative values of the potential V_p applied to a cylindrical probe. It was assumed that the ions started at infinity isotropically with the same energy, and that there was no sheath. That is, the plasma potential V_s (for space potential) varied very gently from the probe to infinity. The ions approaching the probe with large angular momentum would orbit and miss it, while those with small angular momentum would be collected. The ion current could then be given by a very simple formula:

$$I_i = A_p n e \frac{\sqrt{2}}{\pi} \left(\frac{e(V_{s1} - V_p)}{M} \right)^{1/2}, \tag{1}$$

where A_p is the probe surface area, e is the electron charge, M is the ion mass and V_{s1} is a substitute for the space potential. This formula predicts that I_i^2 should vary as V_p, giving a straight line I^2–V plot from which n can be calculated. The intercept V_{s1} of this line is not the real V_s because equation (1) is not valid near V_s, and I_i actually curves near there. Equation (1) is extremely useful because it is independent of both ion energy and the Maxwellian T_e, both of which have canceled out. The density n can be obtained by a simple fitting of this line to the I_{sat} data by adjusting n and V_{s1}. Later, Langmuir extended the theory to Maxwellian ions with a temperature T_i starting from a sheath edge at a radius s. The result was a group of more complicated formulas involving error functions. A series of unreasonable approximations is necessary to reduce this set to equation (1). An attempt [6] to justify equation (1) physically was unsuccessful, but a linear I^2–V plot fits experiment better than all other theories.

Since most plasmas have very small Debye lengths λ_D, a sheath should form around a probe tip, creating an 'absorption radius' inside of which the electric field is so strong that ions inside this radius would be drawn in by an electric field strong enough to prevent any orbiting. The first attempt to treat the case of a thin sheath around a probe was made by Allen *et al* [7] in 1957. This is called the Allen–Boyd–Reynolds (ABR) theory. Ions were assumed to start from infinity with no transverse energy, so that they all traveled radially to the probe. A sheath was formed to partially shield the probe's negative

voltage, and all ions were collected without orbiting. The potential distribution and ion current could be computed from a fairly simple radial differential equation, which originally was for spherical probes but has been extended to cylindrical ones [8].

The neglect of orbiting was too severe a simplification, and in 1958 one of us (FFC) convinced Bernstein to tackle the problem of including both sheath formation and orbiting. The problem was complicated by the fact that orbiting ions contribute twice to the ion density at each radius, while collected ions, whose number is not known beforehand, contribute only once. Bernstein's elegant solution [9] was a two-part differential equation that was computed by Rabinowitz. Monoenergetic ions were assumed to start at infinity isotropically. Extending this to Maxwellian ions with temperature T_i turned out to be a more difficult problem because of numerical instabilities. Laframboise succeeded in this task; his results were given in an unpublished paper [10] and have been summarized by Chen [1, 8]. This is called the Bernstein–Rabinowitz–Laframboise (BRL) theory. The numerical curves have been fitted to algebraic approximations by Steinbruchel [11], Tuszewski and Tobin [12] and Chen [13]. These three theories, orbital motion limited (OML), ABR and BRL, will be used to compute the ion density from measured ion currents.

2. Apparatus

2.1. Plasma source

Experiments were carried out in the chamber shown in figure 1. A PlasmaTherm® inductively coupled plasma (ICP) source is mounted on top of a vacuum chamber lined with small permanent magnets forming a 'magnetic bucket' [14], which helps to confine the plasma drifting down from the source. The three-turn antenna is wound around the periphery of the ceramic source chamber. Though the radiofrequency (RF) energy is deposited only in a thin skin layer near the circumference, the plasma density is almost radially uniform, as shown in figure 2. How this can happen has recently been explained by Curreli and Chen [15]. The antenna is driven at 2 MHz by an RFPP® Model RF10M generator up to 1 kW. Plasma was produced at 300, 450, 600, 750 and 900 W at neutral argon pressures of 1, 2, 5 and 10 mTorr, yielding a matrix of 20 conditions spanning typical conditions in industrial plasma processors.

2.2. Diagnostics

The diagnostic system is shown in figure 3. The Langmuir probe is inserted from the bottom. At the same height, 22 cm below the top plate, a microwave interferometer (MWI) beam is injected across the plasma to measure the line-integrated plasma density by comparing the phase shift between the leg that passes through air and the one that goes through the plasma. The electronics for this are from an HP 8510C network analyzer. Near the Langmuir probe there is also a plasma-oscillation probe (POP) consisting of a hot filament and an antenna connected to a spectrum analyzer. This diagnostic will
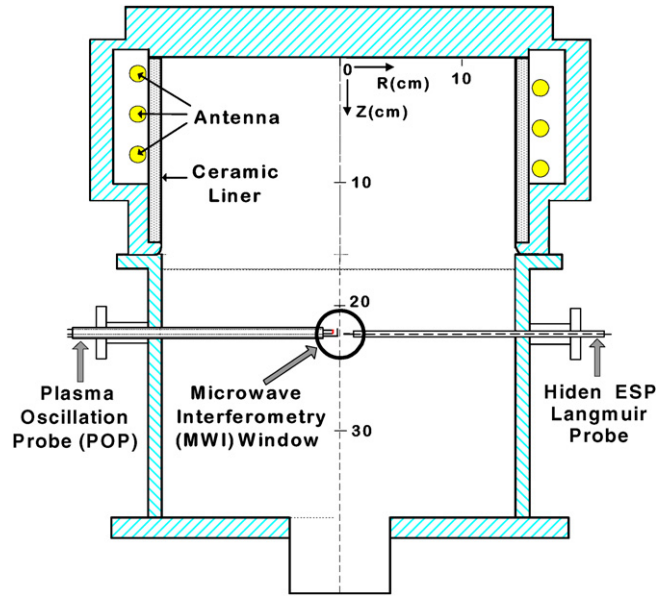

Figure 1. PlasmaTherm® ICP source on top of a magnetic bucket. A 3-turn spiral antenna is wrapped around a ~1 cm thick ceramic liner which contains the plasma it creates when energized with RF. A Hiden ESP® Langmuir probe (right) and the POP (left) are visible through an MWI access window. All diagnostics sample the region $R = 0$, at axial distance $z = 22$ cm from the top of the source. Machine parameters: module I.D. = 32 cm, module-bucket interface at $z = 16.4$ cm, bucket I.D. = 35.5 cm, bucket height = 20.5 cm, RF power $P_{rf} = 300$–900 W, neutral pressure $p_0 = 1$–10 mTorr Ar, plasma density $n = (4 \times 10^{10})$–(5×10^{11}) cm^{-3} and electron temperature $T_e = 2$–4 eV.
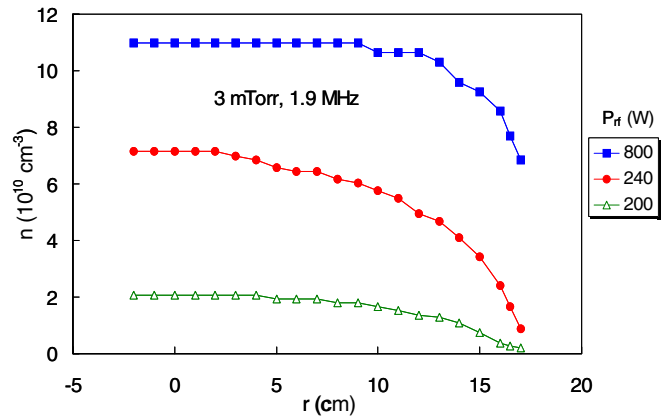
Figure 2. Density profiles in the ICP of figure 1. The density is peaked on axis even though the skin depth of the RF is only 3 cm.

be described later. The MWI and POP measure the electron density, which should be the same as the ion density measured by the Langmuir probe.

The Langmuir probe is the Hiden ESP Mk2® system consisting of a probe, a voltage sweep circuit and software ESPsoft HAL IV® to collect and analyze the data. The probe has a tungsten tip of radius $R_p = 0.075$ mm and length $L_p = 1$ cm and an RF compensation system with RF chokes and a large RF compensation electrode as prescribed by Sudit *et al* [16] The software can apply a cleaning voltage to the probe and take an $I–V$ (current–voltage) curve of several hundred points in a couple of seconds. It can also analyze the data with
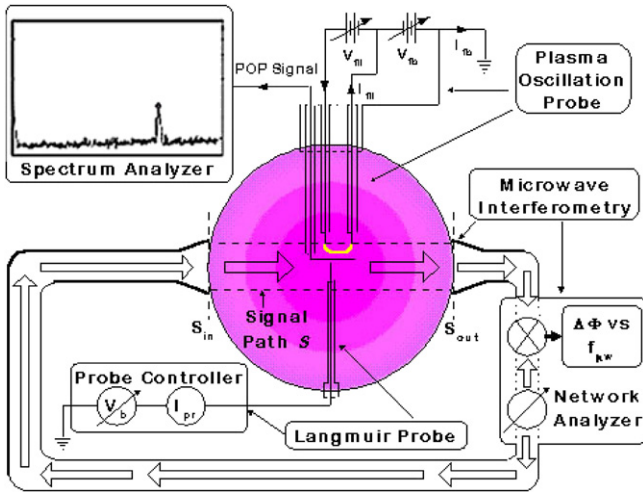
Figure 3. Conceptual cutaway (top) view of experimental setup, including the essential elements of the diagnostics. Also shown (dotted lines) is the plasma volume subtended by the MWI signal beam path, which encompasses the region sampled by the POP and Langmuir probes.

the OML or ABR theory automatically or semi-automatically with user inputs. Our analysis was done, however, with Excel files written by the authors.

3. Measurements

3.1. Langmuir probes

Figure 4 is an example of probe data taken in this experiment. The I^2–V_p (or V) plot in the ion region is close to linear. It is fitted with a polynomial. RF compensation is so good that the $\ln(I_e)$–V_p plot is linear over almost three orders of magnitude, indicating a Maxwellian distribution. The derivative dI/dV, whose minimum should occur at the space potential, shows a well-defined peak. However, not all data are this good in RF plasmas.

A critical parameter is $\xi_p \equiv R_p/\lambda_D$, the ratio of probe tip radius to the Debye length, which determines whether the sheath around the probe is thin or thick, and whether there is an absorption radius. To illustrate how I–V curves change with ξ_p, we next show recent data from a helicon discharge, which can reach higher densities than an ICP.

Figure 5 shows the ion and electron parts of a low-density discharge. We first analyze the data with OML theory. We see that I_i^2 in (a) falls on a straight line, whose least-squares fit yields the density n according to equation (1). The electron current I_e is obtained by subtracting the straight-line I_i *fit* from the total current. The $\ln(I_e)$ versus V_p plot is shown in figure 5(*b*). A Maxwellian distribution appears as a straight line on this plot, since

$$I_e = nev_{\text{the}}e^{(V_p - V_s)/KT_e}, \qquad (2)$$

where v_{the} is the electron random velocity. It is seen that the $\ln(I_e)$ points form a straight line, a fit to which has a slope yielding KT_e, according to equation (2). Since n is already known from I_i (a very convenient feature of the OML formula),

the horizontal position of the fitting line yields V_s. Note that V_{s1} in equation (1) is only the intercept of the ion fit and is not the actual V_s, since $I_i(V_p)$ curves near floating potential V_f and deviates from a straight line there. The behavior of I_i near V_f is immaterial, since n is determined from the points at large negative V_p. The red line in the $\ln(I_e)$ plot gives the raw I_e data before I_i subtraction. An accurate value for KT_e depends on an accurate subtraction of the ion current. Use of this part of the I–V curve is necessary only if RF compensation is insufficient to give a true T_e nearer to V_s.

When the same data are analyzed with the BRL theory (figure 6), the theoretical ion current deviates from a straight line only slightly at the highest $|V_p|$. Both n and T_e agree with the OML analysis because n is low enough that ξ_p is small, and in this limit BRL reduces to OML.

Figure 7 gives the result of ABR analysis of the same data. The $I_i^2 - V_p$ curve is nearly linear, but the density is lower than with OML or BRL. This is always the case because ABR neglects orbiting and expects the collected current to come straight from a lower density plasma. In the BRL and ABR analyses, I_i depends on T_e, and iteration between the two graphs is necessary to get fits in both of them.

We next show examples at high density, where $\xi_p \gg 1$. Figure 8 shows I_{sat} for a density above $10^{12}\,\text{cm}^{-3}$, fitted to OML theory. The data have a slight curve but can be fitted will with a straight line.

Figure 9 shows the BRL analysis of the same data. The theoretical curve does not fit the data very well, and the best fit yields a much higher density than OML gives. At values of $\xi_p \gg 1$, an absorption radius should form, thus distorting the straight line. The high ion current is caused by collisions which interrupt the orbiting outside the absorption radius, as we shall discuss later. Figure 10 shows the ABR analysis of the same data. It is known [8] that the ABR curves for cylinders follow an I^2–V law for ξ_p smaller than about 3, and this fit is seen in figure 10. However, the calculated I_i extends into the electron region, making ion subtraction impossible. The density calculated from the large $|V_p|$ region is lower than the OML density, as is expected when orbiting is neglected. The range of densities in the current experiment is in an intermediate range, where the theoretical curves are neither very similar nor very hard to fit to the data.

3.2. Microwave interferometry

This diagnostic technique has been described in books [17, 18]. The klystron and other electronic components have in this case been replaced by a Hewlett-Packard 8510C® vector network analyzer. The microwave beam is launched from one microwave horn and received by another, diametrically opposite, horn, sampling the same plasma probed by the other diagnostics (figure 3). The phase of the received signal is compared with that of the internal generator. A 360° phase change constitutes one 'fringe'. Without plasma, a transit across the chamber yields a phase shift of about 10 fringes at our microwave frequency f_0 of ≈88 GHz. In the presence of plasma, the microwave's wavelength λ_0 is about 1% longer at our densities, resulting in a fringe shift of about 0.1 fringe

(a)

(b)

(c)

(d)
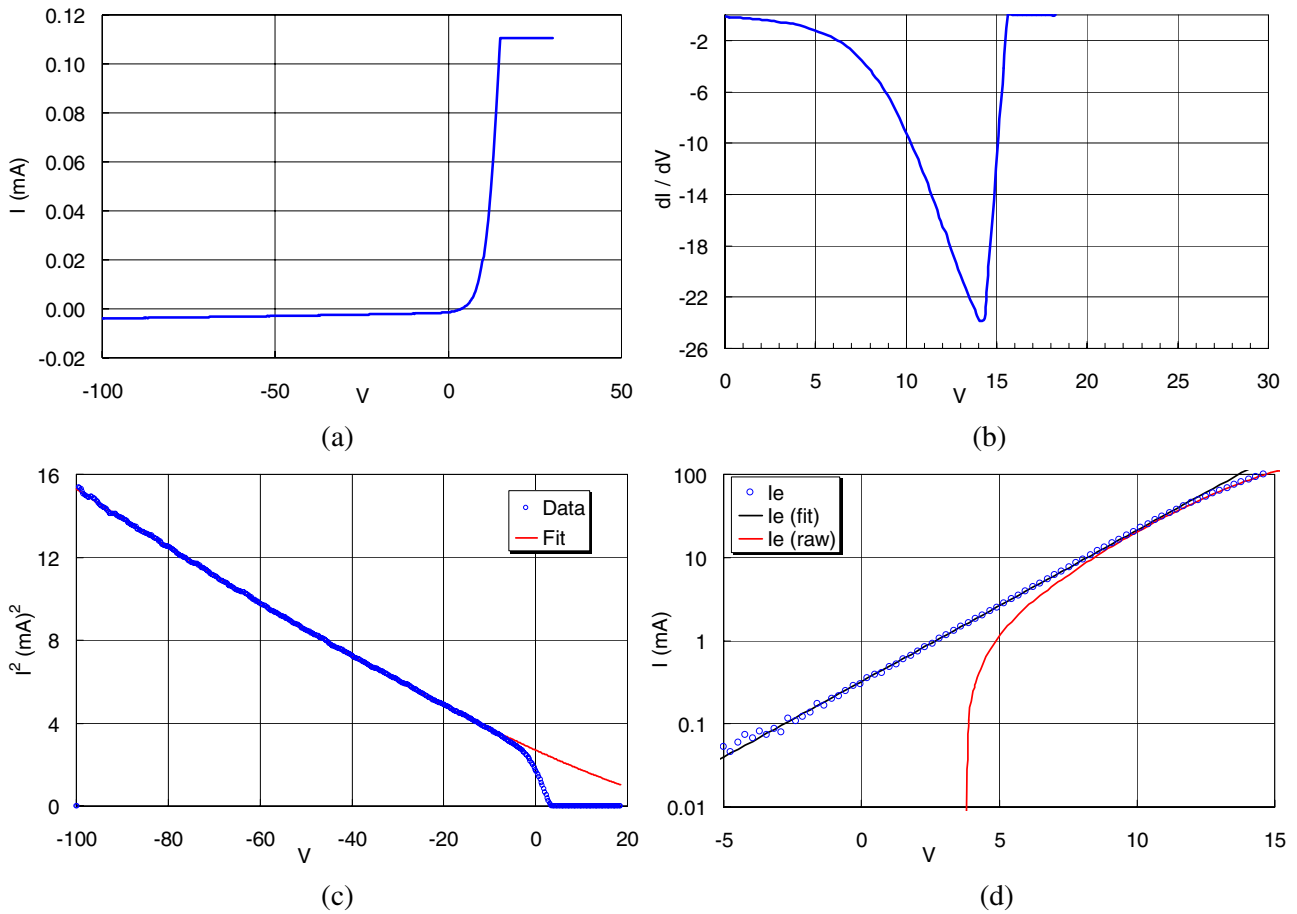
Figure 4. (*a*) Entire I–V curve; (*b*) derivative of I–V curve with a sharp minimum indicating the plasma potential; (*c*) plot of I_i^2 versus V_p (points) and straight-line fit (——); (*d*) semilog plot of I_e versus V_p and straight-line fit to a Maxwellian.


(a)

(b)
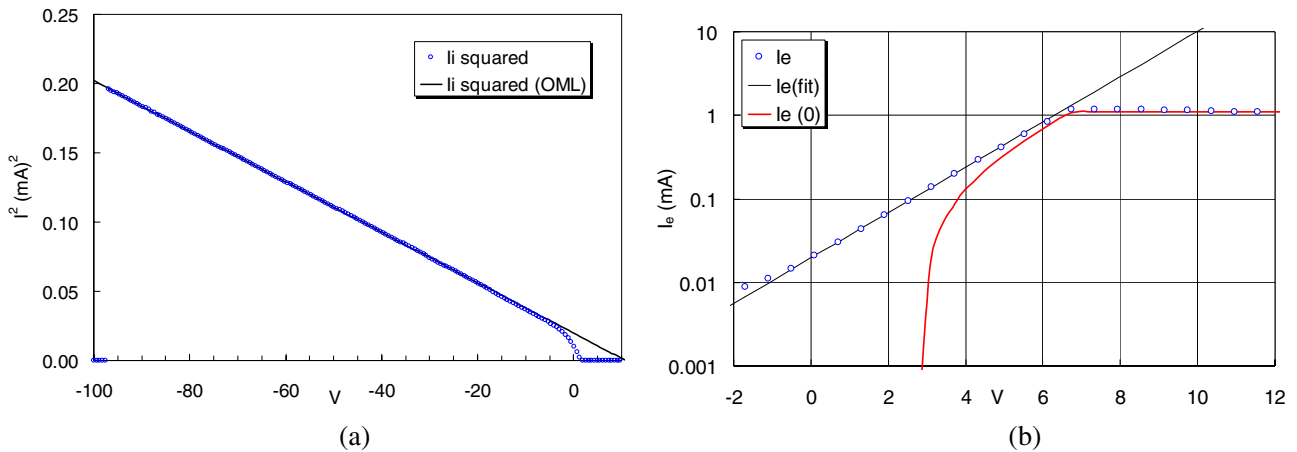
Figure 5. (*a*) Plot of I_i^2 versus V_p as in figure 4(*c*). (*b*) Semilog plot of I_e versus V_p and a Maxwellian fit, as in figure 4(*d*). For convenience the I_e data were taken only up to 1 mA. The OML result is $n = 0.80 \times 10^{11}$ cm^{-3} and $KT_e = 1.60$ eV ($\xi_p = 1.92$).

relative to vacuum. This is a 36° fringe shift, which can be measured to $\approx 1\%$ by the network analyzer, whose basic accuracy is 0.05 dB in amplitude and 0.5° in phase.

Several sources of error have to be avoided. Diffraction of the beam can occur if the windows are not much larger than λ_0. In this case, the window diameter is 26.6 mm, much larger than a λ_0 of ≈ 3.5 mm. Refraction of the beam by plasma gradients would occur if these gradients are comparable to λ_0.

Here the plasma radius of ≈ 180 mm is much larger than λ_0, and the plasma is quite uniform (figure 2) besides. Reflection of the beam from curved walls can cause multipath signals to be detected. The chamber is so large compared with λ_0 that its curvature can be neglected as long as the beam is directed along a diameter. To avoid electron plasma effects, f_0 should be much larger than the electron plasma frequency f_p. An $f_0 \approx 88$ GHz is an order of magnitude above f_p at our highest
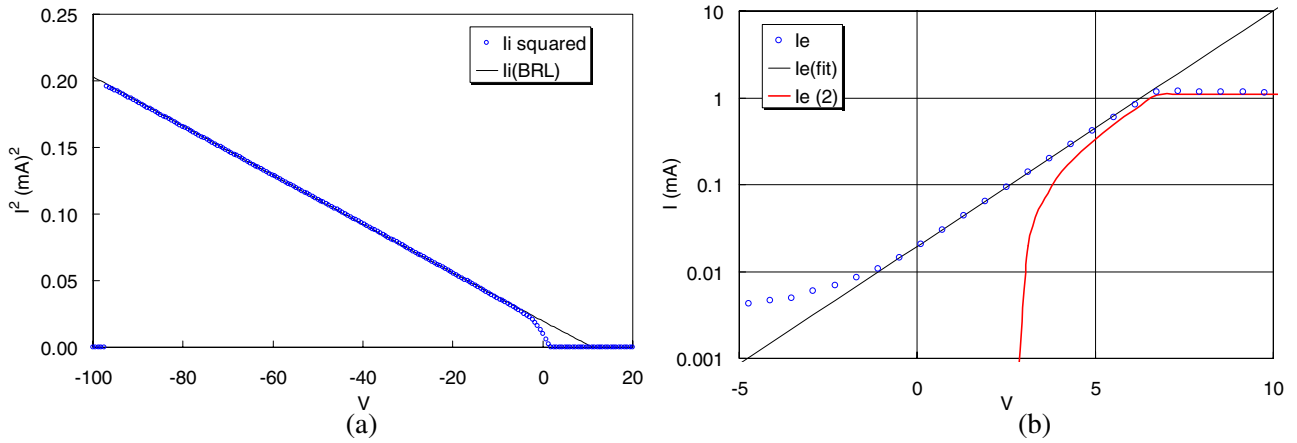
Figure 6. Same data as in figure 5 but analyzed with the BRL theory. The result is $n = 0.81 \times 10^{11}$ cm^{-3} and $KT_e = 1.60$ eV ($\xi_p = 1.93$).
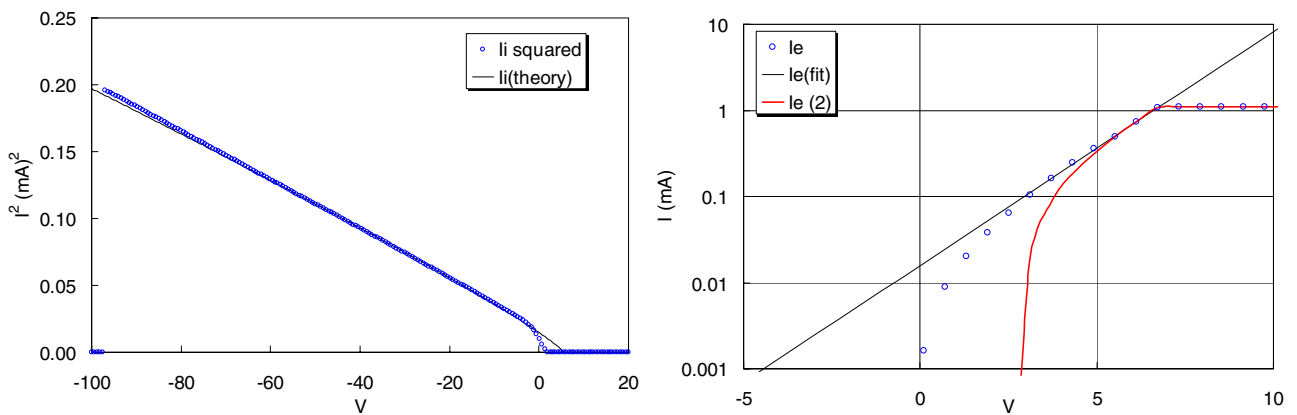
Figure 7. Same data as in figure 4 but analyzed with the ABR theory. The result is $n = 0.23 \times 10^{11}$ cm^{-3} and $KT_e = 1.60$ eV ($\xi_p = 1.03$).
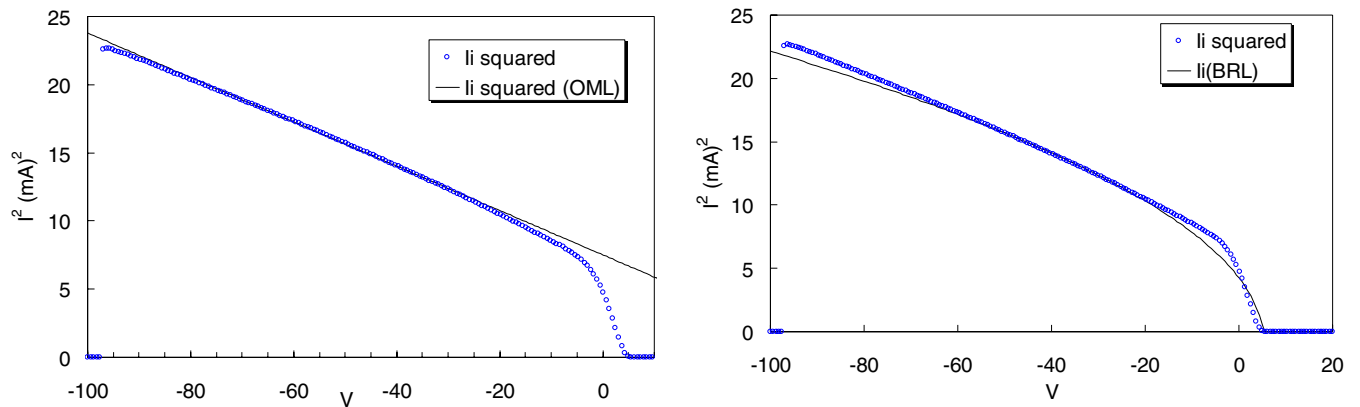
Figure 8. An OML fit to the ion current in a high-density plasma. The result is $n = 1.3 \times 10^{12}$ cm^{-3} and $KT_e = 3.0$ eV ($\xi_p = 5.6$).
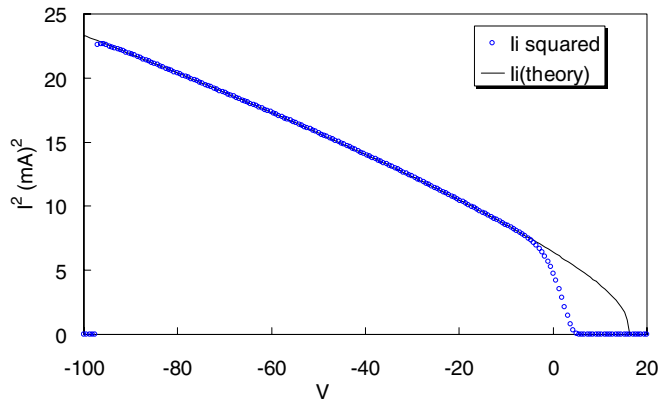

Figure 9. A BRL fit to the same data as in figure 8. The result is $n = 3.4 \times 10^{12}$ cm^{-3} and $KT_e = 2.6$ eV ($\xi_p = 9.9$).

density of $<10^{12}$ cm^{-3}. To ensure that none of these resonant effects occurs, we swept f_0 from 82 to 88 GHz. Figure 11 shows the density inferred from the microwave fringe shift versus f_0. There are no spurious effects.

Microwave interferometry (MWI), of course, measures only the line-integrated density. To get the local density, one has to do an Abel inversion using the probe-measured $n(r)$ and assuming azimuthal symmetry. This was done, but it was not really necessary, since $n(r)$ is so uniform, as shown in figure 2.
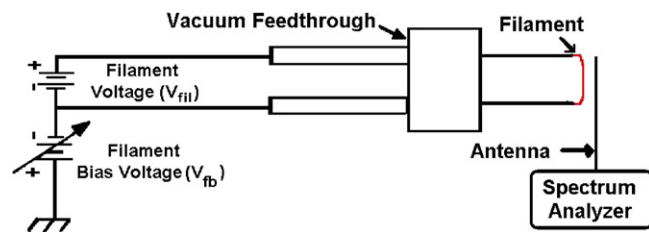
3.3. Plasma-oscillation probe

This diagnostic, developed by Sugai and collaborators [19], measures n_e by exciting electron plasma oscillations, whose frequency ω_p directly yields n_e. Following Sugai, we built the apparatus shown in figure 12 and placed it as close as possible to the Langmuir probe. A tungsten filament is heated to electron emission by the upper power supply, and it is biased to a large negative voltage V_{fb} by the lower supply. A beam of electrons

Figure 10. An ABR fit to the same data as in figure 8. The result is $n = 1.06 \times 10^{12}\,\mathrm{cm}^{-3}$ and $KT_e = 2.3\,\mathrm{eV}$ ($\xi_p = 5.8$).
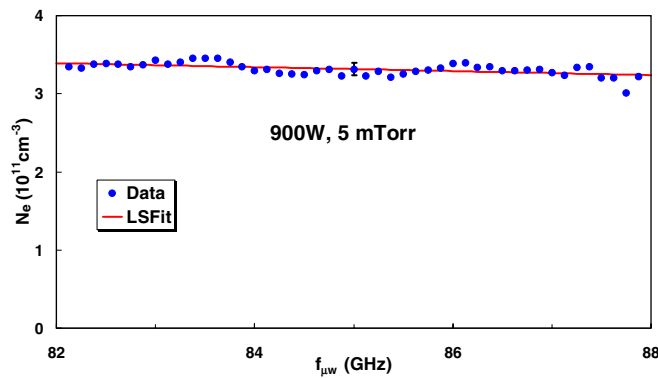
Figure 11. Plasma density measured by MWI at various frequencies, showing absence of spurious effects.


Figure 12. Diagram of POP apparatus.

of energy eV_{fb} is then ejected into the plasma. If the beam's energy and current are large enough, it will excite plasma oscillations via the beam-plasma instability. These oscillations are detected by an antenna and sent to a spectrum analyzer, which measures their frequency. Near threshold, the spectrum will be a narrow peak, as shown by the inset in figure 3. Overdriving the instability will result in a wider spectrum and possible harmonics and beats. From a narrow peak, the density can be calculated from the usual formula $\omega_p^2 = n_e e^2 / \varepsilon_0 m$.

4. Results

The data shown here were taken in the machine shown in figure 1. The RF frequency was 2 MHz, and the probes were in the quiescent plasma below the ICP source where the RF amplitude was small and the Langmuir probe has sufficient
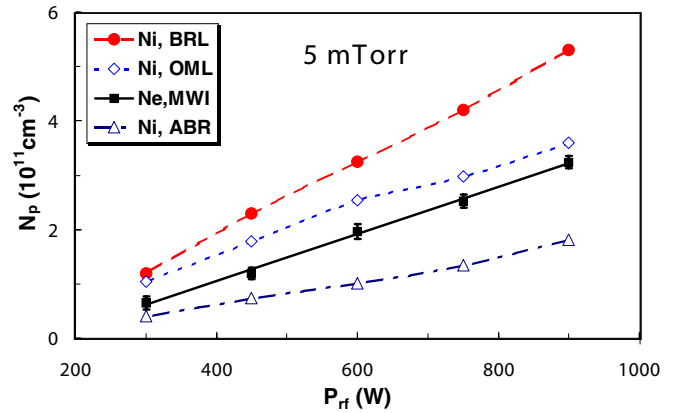
Figure 13. Plasma density measured with MWI (solid black line), compared with probe data analyzed with various theories.
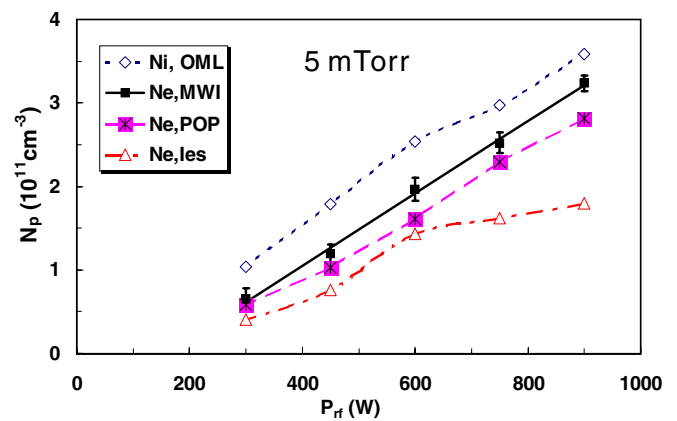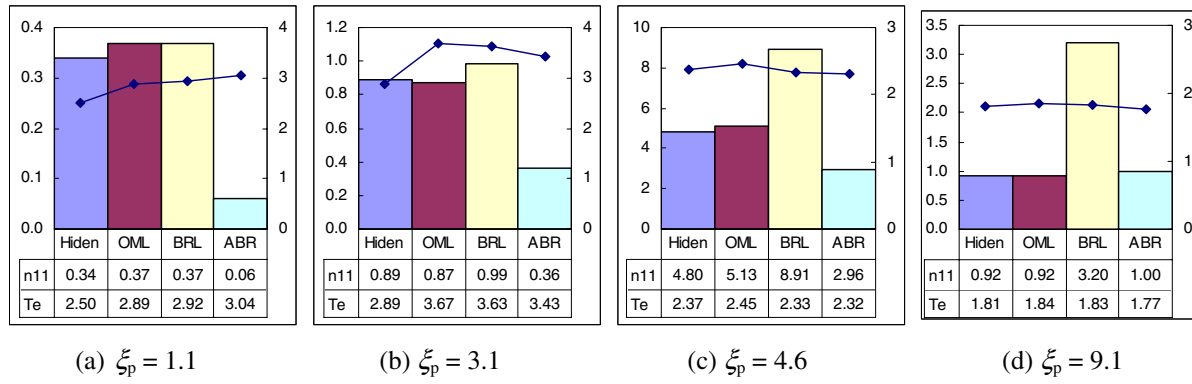

Figure 14. The data of figure 13 compared with n_e from POP and electron saturation current I_{es}.

RF compensation to allow T_e measurements up to the space potential. Figure 13 shows a power scan of the density at 5 mTorr of argon, as analyzed by the OML, BRL and ABR theories. In this case, the OML theory happens to agree best with the real density from MWI. The fact that BRL greatly overestimates and ABR greatly underestimates the plasma density agrees with results of other authors before and after this work. Figure 14 shows the same data with the addition of POP and I_{es} results, where I_{es} is obtained from the electron saturation current. The latter is not to be trusted in industrial plasmas because it can be affected by collisions, magnetic fields, or potential pulling by the probe. The last effect occurs when the electron current is so large that it can make the potential of the entire plasma more positive if the plasma is not in contact with grounded walls. If saturation electron current is drawn in too long a pulse at high density, the probe tip can be heated to emission.

That the disagreement among theories depends on ξ_p is illustrated in the four sample cases in figure 15. These were taken in different plasmas and with different probe radii. The T_e values do not vary much, but the n values show great differences. The 'Hiden' data also use OML, and differ from 'OML' only in the fitting ranges chosen by the automatic ESP® analysis.

Figure 16 shows the ratio of BRL-to-OML and ABR-to-OML determined densities for all test cases. ABR is always

6

	Hiden	OML	BRL	ABR
n11	0.34	0.37	0.37	0.06
Te	2.50	2.89	2.92	3.04

(a) $\xi_p = 1.1$

	Hiden	OML	BRL	ABR
n11	0.89	0.87	0.99	0.36
Te	2.89	3.67	3.63	3.43

(b) $\xi_p = 3.1$

	Hiden	OML	BRL	ABR
n11	4.80	5.13	8.91	2.96
Te	2.37	2.45	2.33	2.32

(c) $\xi_p = 4.6$

	Hiden	OML	BRL	ABR
n11	0.92	0.92	3.20	1.00
Te	1.81	1.84	1.83	1.77

(d) $\xi_p = 9.1$

Figure 15. Comparison of ion collection theories in four plasmas with different values of ξ_p. Bars show n in units of 10^{11} cm^{-3} on the left scale; points show KT_e on the right scale.
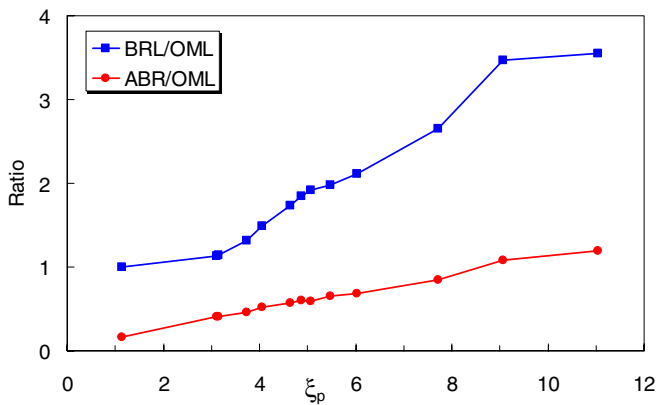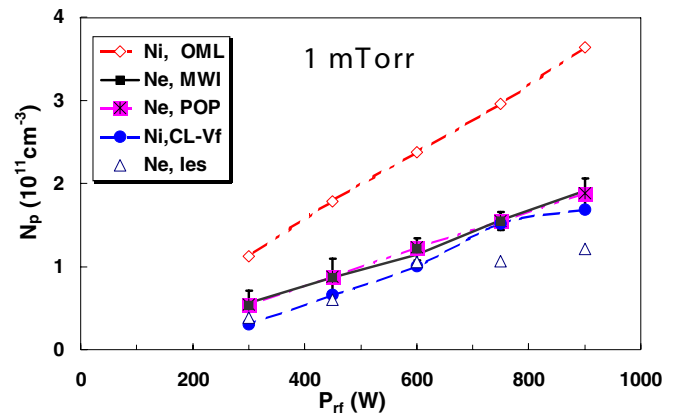

Figure 16. Ratio of densities determined by different theories as a function of ξ_p calculated from the OML density.

Figure 17. Power scan of density at 1 mTorr with various diagnostics, taken on axis ($r = 0$).

Figure 18. Power scan of density at 2 mTorr with various diagnostics.

lower, and BRL is always higher. The BRL/OML ratio gets higher than 3 here but has reached as high as 7 in all our tests. Further data can be found in [13].
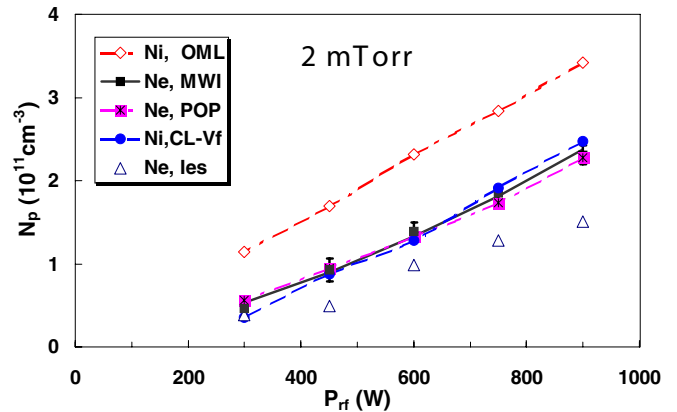
The entire matrix of calibrations at four pressures and five RF powers is summarized in figures 17–20. The OML, MWI and POP diagnostics were described above. The CL-V_f points are computed with a new Child–Langmuir (C–L)-floating potential method presented in the next section. This method agrees best with the true density measured by MWI and POP. The I_{es} points are from saturation electron current and can be accurate only in laboratory plasmas but not in normal industrial plasmas. The OML method, which is used in most commercial probe systems, fails at low pressures because it predicts too many orbiting ions which do not reach the probe. At higher pressures, collisions with neutrals destroy some of the orbiting and bring OML closer to the correct result accidentally. This effect will be discussed later.

5. Discussion

Langmuir probes can be designed to be 'thick' or 'thin'. Thick probes have $R_p \gg \lambda_D$ so that the sheath is thin, and the sheath area is not much larger than the probe area A_p. In that case, the ion current is approximated by [1] $A_p \alpha_0 nec_s$, where

$\alpha_0 \approx \frac{1}{2}$ and c_s is the 'Bohm velocity', equal to the ion acoustic velocity $(KT_e/M)^{1/2}$ in a single-species plasma. Thick probes, however, have to be long enough to approximate an infinite cylinder and therefore may draw enough current to disturb the plasma. Also, thick probes may become 'thin' at low densities. This paper emphasizes the more commonly used thin probes, but these suffer from difficulties in calculating ion orbits in the presence of finite sheath thicknesses. Many theories are
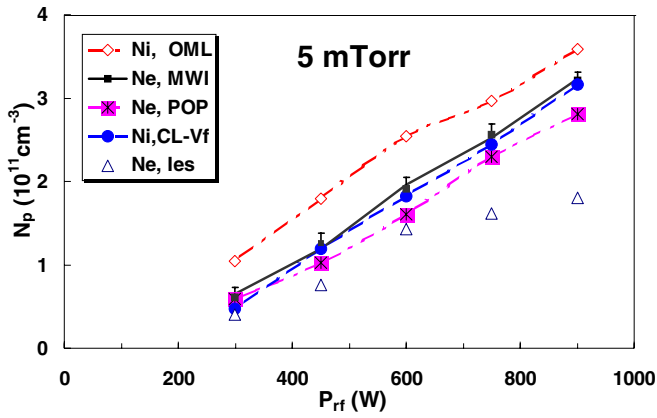
Figure 19. Power scan of density at 5 mTorr with various diagnostics.
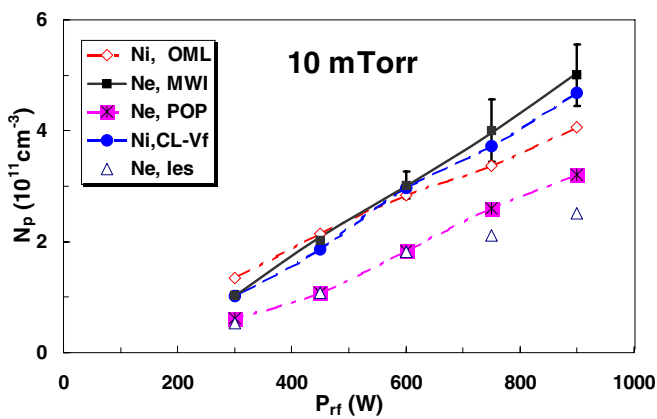
Figure 20. Power scan of density at 10 mTorr with various diagnostics.

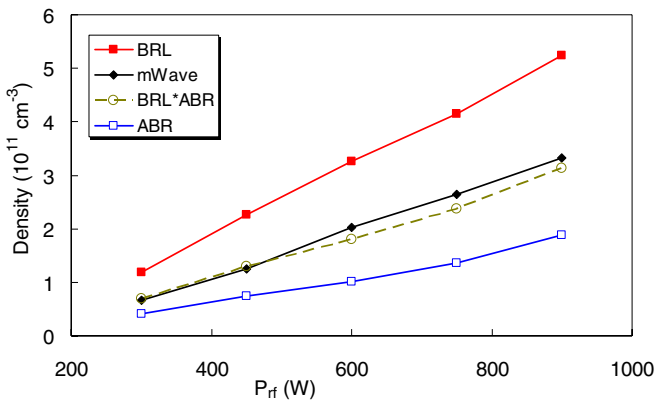**Figure 21.** Example of the agreement of the geometric mean (–○–) between BRL and ABR and the MWI density.

limited to spherical probes because of logarithmic divergences in cylindrical geometry, but spherical probes are impractical in experiment. To reconcile probe data with calibrations, one can take the geometric mean between the BRL and ABR results. The agreement is shown in figure 21. However, this is cumbersome, since it requires two fits for each point.

The CL-V_f theory is intermediate between 'thick' and 'thin' and fits the microwave data best. This idea came about

because some I_i–V curves fit better when $I^{4/3}$ is plotted against V_p rather than I^2, as seen in figure 22.

The $V^{3/4}$ dependence of I_i is reminiscent of the C–L law [20, 21] for pure ion sheaths:

$$I_i = \frac{4}{9}\left(\frac{2e}{M}\right)^{1/2}\frac{\varepsilon_0|V - V_s|^{3/2}}{d^2}, \tag{3}$$

where d is the thickness of the C–L sheath and varies as $|V_p - V_s|^{3/4}$. The value of I_i at $V = V_f$ is easily found from figure 22, since V_f is the voltage where the data points go to zero, and the straight-line fit to I_i is only a short extrapolation to V_f. Knowing $I_i(V_f)$ and V_f, we can solve equation (3) for d. The result is

$$d = 1.018\eta_f^{3/4}\lambda_D, \tag{4}$$

where $\eta_f \equiv |V_s - V_f|/KT_e$, $\lambda_D \equiv (\varepsilon_0 KT_e/ne^2)^{1/2}$.

We now assume that the absorption radius of the probe lies a distance d from the probe surface, so that a probe of radius R_p and length L collects a current

$$I_i(V_f) = 2\pi(R_p + d)L\alpha_0 nec_s. \tag{5}$$

The density n appears linearly here and also as $n^{-1/2}$ in d. Equation (5) is thus a quadratic equation in $\sqrt{n}$ which can easily be solved to obtain n. This is the value labeled N_i, CL-V_f in figures 17–20. This floating-potential method is explained in detail by Chen *et al* [22], including the fact that it is empirical and has no rigorous theoretical foundation.

Though we have shown empirical methods to obtain values of n from probe data that agree with microwave measurements, the question remains as to why the ABR and BRL theories are so erroneous. It is clear that ABR cannot be applied to thin probes because it neglects ion orbiting. That BRL overestimates n, we believe, is due to the fact that collisions are neglected. When an orbiting ion makes a collision with a neutral atom, it charge-exchanges and loses its angular momentum. It then moves radially into the probe rather than misses it. Thus I_i is larger, and the theory expects a higher density.

The effect of collisions on ion current collection has been considered by many authors, but mostly for spherical probes. The early work of Self and Shih [23] was a careful extension of ABR to include collisions. Delicate spherical probes were constructed, and comparison was made with a microwave cavity. The experiment was in a small dc discharge at low density. Wasserstrom and Su [24] included orbiting by dividing phase space in two and using a different distribution function in each. Chou *et al* [25] worked out the kinetic theory of a spherical probe with collisions, but the equations could not be solved, and the effect was a collisional *decrease* of ion current, not the orbiting effect. Treatments of the continuum problem, in which ions moved by diffusion with short mean free paths, were comparatively simple. Bienkowski and Chang [26] included orbiting, using a moment method to derive equations for intermediate collisionality which reduced to the known collisionless and continuum limits.
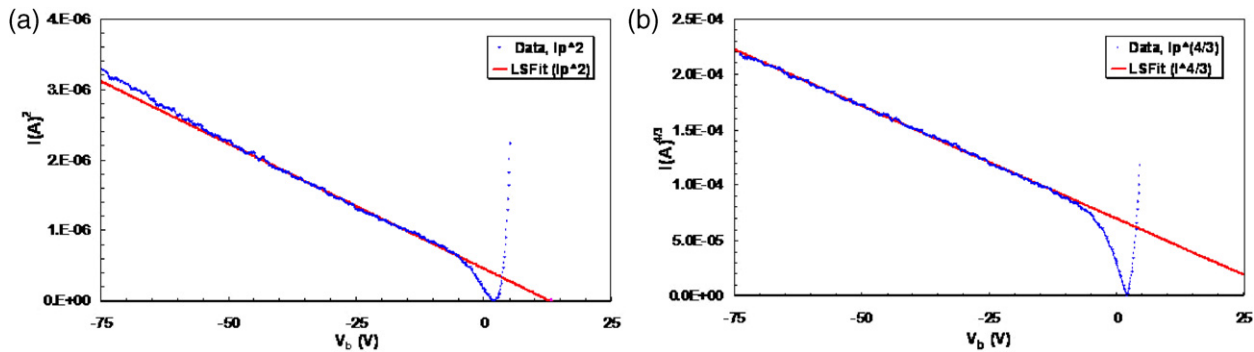
Figure 22. Ion curves (*a*) I^2–V and (*b*) $I^{4/3}$–V, showing a better fit with $I^{4/3}$.

There have been two books on probes. In Swift and Schwar [27], BRL orbiting was not treated. Chung *et al* [28] is the better reference for the continuum case. They also give a good summary of the attempts cited above to treat the case of intermediate collisionality. In more recent times, Knappmiller *et al* [29] compared *cylindrical* probe, disc probe, microwave cavity and microwave hairpin measurements at 10^8 cm^{-3} densities in a dc plasma and noted the effects of collisions. However, no general theory was given that could be used at higher densities. Going back to spheres, Lampe *et al* [30] considered collisions, but only with application to the charging of spherical dust particles. Hutchinson and Patachini [31] calculated ion currents with collisions, but again only for spheres.

6. Conclusions

We have compared a Langmuir probe with microwaves for local density *n* measurements in industrial RF plasmas which are not collisionless. Different theories were used to interpret the probe *I*–*V* characteristics. We find that the BRL theory greatly overestimates the plasma density, while the ABR theory underestimates it. Langmuir's original OML theory works best if the probe is made as thin as possible to decrease $\xi_p \equiv R_p/\lambda_D$. This gives *n* to within a factor of 2 except at very low pressures of argon. Such a probe can be used successfully up to the high 10^{12} cm^{-3} range in RF plasmas as long as one understands that the value of *n* may be somewhat inflated. A new floating-potential method is proposed which agrees well with microwave densities, but the method has no theoretical justification. What is needed is a theory for cylindrical probes which includes ion orbiting and intermediate collisionalities.

Acknowledgments

This experiment was conducted during a one-week visit by WZ from Hiden Analytical, Ltd, around the year 2000. The results were written by JDE in a detailed paper [32] in 2001. A sampling of the data taken by JDE and WZ was published previously [13]. The entire set is presented in this paper. FFC is grateful for WZ's instigation of this experiment and for JDE's analysis of the results. This work extends an earlier study by Tuszewski and Tobin [12] which used low-frequency RF discharges in which compensation for RF pickup was

difficult. They found probe-derived densities to be a factor of 2–3 higher than those from microwave interferometry but could not eliminate RF interference as the cause.

The authors thank Hiden Analytical, Inc., for sending WZ to our laboratory and for the use of their probe in this work. We are indebted to Brendan Melia of Hiden and F Matt Espiau of the UCLA Center for High Frequency Electronics for their valued technical support. We are also grateful to Dave Johnson and John Donohue of PlasmaTherm® (now Unaxis®) for the use of their ICP source module.

References

[1] Chen F F 1965 Electric probes *Plasma Diagnostic Techniques* ed R H Huddlestone and S L Leonard (New York: Academic) pp 113–200 chapter 4
[2] Hershkowitz N 1989 How Langmuir probes work *Plasma Diagnostics* vol 1 ed O Auciello and D L Flamm (Boston, MA: Academic) chapter 3
[3] Swift J D and Schwar M J R 1970 *Electrical Probes for Plasma Diagnostics* (London: Iliffe Books)
[4] Chung P L, Talbot L and Touryan K J 1975 *Electric Probes in Stationary and Flowing Plasma* (Berlin: Springer)
[5] Mott-Smith H M and Langmuir I 1926 *Phys. Rev.* **28** 727
[6] Chen F F 2009 *Plasma Sources Sci. Technol.* **18** 035012
[7] Allen J E, Boyd R L F and Reynolds P 1957 *Proc. Phys. Soc.* (Lond.) B **70** 297
[8] Chen F F 1965 *J. Nucl. Energy* Pt. C **7** 47
[9] Bernstein I B and Rabinowitz I N 1959 *Phys. Fluids* **2** 112
[10] Laframboise J G 1966 University of Toronto Institute for Aerospace Studies *Report* 100, unpublished
[11] Steinbruchel C 1990 *J. Vac. Sci. Technol.* A **8** 1663
[12] Tuszewski M and Tobin J A 1996 *Plasma Sources Sci. Technol.* **5** 640
[13] Chen F F 2001 *Phys. Plasmas* **8** 3029
[14] Limpaecher L and MacKenzie K R 1993 *Rev. Sci. Instrum.* **44** 426
[15] Curreli D and Chen F F 2011 *Phys. Plasmas* **18** 113501
[16] Sudit I D and Chen F F 1994 *Plasma Sources Sci. Technol.* **3** 162
[17] Heald M A and Wharton C B 1965 *Plasma Diagnostics with Microwaves* (New York: Wiley)
[18] Chen F F 1984 *Introduction to Plasma Physics and Controlled Fusion vol 1: Plasma Physics* 2nd edn (New York: Plenum) p 118
[19] Shirakawa T and Sugai H 1993 *Japan. J. Appl. Phys.* **32** 5129
[20] Lieberman M A and Lichtenberg A J 2005 *Principles of Plasma Discharges and Materials Processing* 2nd edn (Hoboken, NJ: Wiley-Interscience) p 176

[21] Chen F F 1984 *Introduction to Plasma Physics and Controlled Fusion vol 1: Plasma Physics* 2nd edn (New York: Plenum) p 294
[22] Chen F F, Evans J D and Arnush D 2002 *Phys. Plasmas* **9** 1449
[23] Self S A and Shih C H 1968 *Phys. Fluids* **11** 1532
[24] Wasserstrom E and Su C H 1965 *Phys. Fluids* **8** 56
[25] Chou Y S, Talbot L and Willis D R 1966 *Phys. Fluids* **9** 2150
[26] Bienkowski G K and Chang K W 1968 *Phys. Fluids* **11** 784
[27] Swift J D and Schwar M J R 1970 *Electrical Probes for Plasma Diagnostics* (London: Iliffe Books)
[28] Chung P L, Talbot L and Touryan K J 1975 *Electric Probes in Stationary and Flowing Plasma* (Berlin: Springer)
[29] Knappmiller, Robertson S and Sternovsky Z 2006 *IEEE Trans. Plasma Sci.* **34** 786
[30] Lampe M, Goswani R, Sternovsky Z, Robertson S, Gavrishchaka V, Ganguli G and Joyce G 2003 *Phys. Plasmas* **10** 1500
[31] Hutchinson I H and Patacchini L 2007 *Phys. Plasmas* **14** 013505
[32] Evans J D, Zawalski W and Chen F F 2011 *Evaluation of Langmuir probe ion density measurement in weakly ionized discharges using plasma oscillation probes and microwave interferometry UCLA Report* LTP-111